Dual mode SDOCT-HSI approach for cancer surgery guidance

D. SAVASTRU[a], S. MICLOS[a], N. IFTIMIA[b], M. A. CALIN[a], R. SAVASTRU[a], D. MANEA[a], S. DONTU[a]
aNational Institute of R&D for Optoelectronics - INOE 2000, 409 Atomistilor St., Magurele, Ilfov, RO-077125, Romania
bPhysical Sciences, Inc., 20 New England Business Ctr. Drive, Andover, MA-01810, USA

An innovative approach for guiding cancer surgery is proposed in this paper. Spectral-Domain Optical Coherence Tomography (SDOCT) and Hyperspectral Imaging (HSI) are combined with the goal of taking advantage of the complementary capabilities provided by each technique: spatial (3D) information at the micron scale and spectral signatures of the biological specimens. The proposed approach offers the potential to solve a major dilemma that every surgeon has to address in the operating room: "are surgical margins free from any outbreak of cancer?". Preliminary results of this work on excised specimens indicate that combined SDOCT-HSI imaging enables reliable detection of cancer presence and therefore it might be used in the future as a clinical tool for differentiating positive margins during surgery.

1. Introduction

Assessment of surgical margins is currently very difficult, almost impossible, to be made intraoperatively. The margin is defined as the distance from the tumour to the cut surface of the specimen. In the management of cancer it is extremely important to achieve negative margins around the primary tumour. The consensus among most of the surgeons and radiation oncologists is that there should be no tumour left within at least 1-2 mm distance from the surface of the surgical specimen [1-3].

Traditionally, surgical specimens are sent to the pathology lab, sectioned, stained, and read for results days later, after the patient has gone home. If a positive margin is left behind, there is a major risk for tumour recurrence, and the patient has to have a second surgery [1-5].This is a tremendous emotional cost for both the patient and the family members.

Current techniques for intraoperative pathologic assessment of surgical margins involve touch prep and frozen section analysis. Cancer specimens however, have a high percentage of fat or necrotic tissue, and thus they are very difficult to freeze and cut in thin slices for histopathological analysis during the surgery. Therefore, the surgical specimen is sent to the pathology laboratory, fixed, sectioned, stained, and read for results days later, after the patient has gone home. Touch prep analysis has a poor sensitivity and specificity, and therefore is not very used. A survey of breast surgeons found that no intraoperative assessment is performed in over 50% of patients (both touch prep and frozen section are sparsely used) [5]. Published reports indicate a 20-70% rate of positive margins left after lumpectomy [6]. Therefore, repeated surgery is needed in all patients left with positive margins.

Based on these observations, it is clear that a better technology is needed in the surgical suite. Such a technology, able to highlight the presence of positive margins, will likely reduce the potential for cancer recurrence.

Several technologies were investigated for addressing this problem. They include micro CT [7,8] and MRI [9,10], as well as radio-frequency spectrometry. However, MRI and micro CT do not provide a cellular-level picture of the tissue microstructure necessary to assess cancer presence on the margins. Radio-frequency spectrometry, has limited sensitivity (70% or less) for positive margins and can only investigate relatively small surface areas (2 mm) [11].

More recently, optical investigation of the surgical bed has been evaluated. Optical methods include optical coherence tomography (OCT) [12], fluorescence imaging [13] and hyperspectral imaging (HSI) [14-19]. However, no optical imaging modality alone was able to reliably detect positive surgical margins.

In this paper we present the combined use of Spectral-Domain Optical Coherence Tomography (SDOCT) and hyperspectral imaging (HSI) for cancer differentiation. Our study shows that the complementary data provided by these two technologies can be processed to provide more reliable evaluation of surgical margins.

2. Materials and methods

2.1. SDOCT-HSI Technology

The proposed approach in this paper is to combine two techniques within the same optical instrument: Spectral-Domain Optical Coherence Tomography and Hyperspectral Imaging.

The reason for using this combination is that SDOCT provides micron-scale 3D spatial information, depicting tissue morphological changes, while HSI provides simultaneously 2D and spectral information depicting changes in biospecimen spectral signatures. Thus 4D (x, y, z and λ) information can be obtained for the investigated sample using the proposed dual-mode approach.

Optical Coherence Tomography imaging consists in the acquisition of tissue reflectivity profiles while scanning a beam across the tissue surface (see Fig. 1). The SDOCT approach has the particularity that the tissue reflectivity is determined by taking the Fourier transform of the light interference pattern that is split into its frequency components by a spectrometer [12]. Therefore, no moving elements are used to gather information from different depths of the sample.
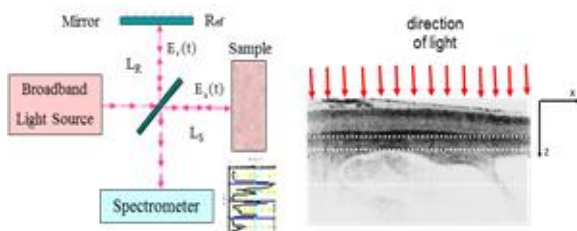

Fig. 1. SDOCT simplified diagram.

The two light beams combine constructively only if the light path difference, L_S-L_R on figure, is within the coherence length of the light source. The coherence length is dependent on the resolution of the interferometer, while the axial resolution is dependent on the bandwidth of the light source: the larger the bandwidth, the better is the resolution [20].

Hyperspectral Imaging consists of an acquisition of a series of images in many adjacent narrow spectral bands and reconstruction of reflectance spectrum for every pixel of the image [21]. The set of images thus obtained (typically tens or hundreds of images) is called the hypercube (Fig. 2). The image hypercube has three dimensions: two dimensions represent the spatial coordinates of a pixel and one dimension gives the wavelength of a particular spectral band.

The principle of hyperspectral imaging is schematically illustrated in Fig. 3. The image of the sample is formed by a lens onto the entrance slit of a spectrograph. Thus only a line of the sample image is selected once. The spectrograph produces a spectrum imaged on a focal plane array detector (a CCD camera), preserving the location of respective points on the slit and thus the points of the line on the sample. Successive lines on the sample are acquired by using a scanning mirror, synchronized with camera frame acquisition.
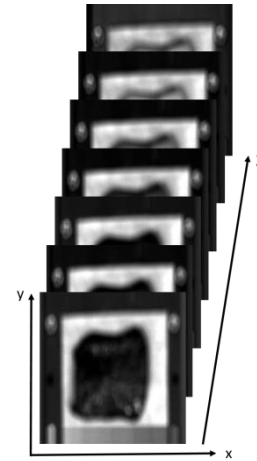

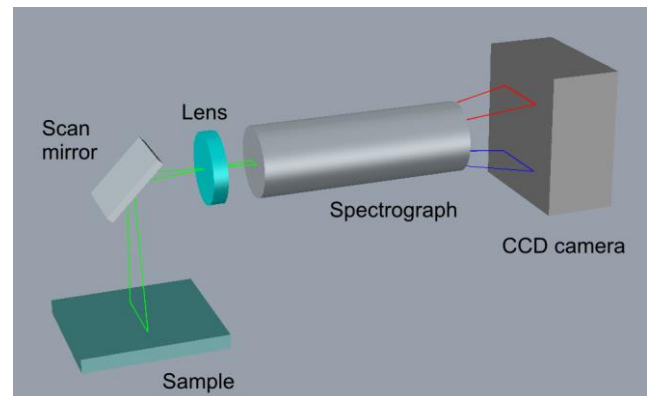*Fig. 2. Schematic representation of a hypercube.*

Fig. 3. Hyperspectral imaging.

2.2. Instrumentation

A simplified schematic of the instrument used in this study, which combines OCT and HSI within the same optical path, is presented in Fig. 4a, while a photograph of the instrument is presented in Fig. 4b.

The SDOCT unit is based on a fibre-optic interferometer and a spectrometer. It uses as a light source a wideband super luminescent diode (Model EXS210046-01, EXALOS, Switzerland) emitting at 1313.3 nm, with a spectral width of 81.3 nm. A circulator (CIR1310-APC from ThorLabs, USA) is used to maximize light collection. The fibre interferometer is made of a 10/90 fibre splitter (Model FC1310-70-10-APC, ThorLabs, USA) which divides the light in two arms: the reference arm (the 10 % terminal) and the sample arm (the 90 % terminal). On the

reference arm the light is collimated by a lens (model F280APC-C, ThorLabs, USA) and reflected back by a mirror. On the sample arm the light is collimated by another collimator (Model F240APC-C, ThorLabs, USA) and sent to the OCT-scanning engine (2D-galvanometer, Model GVSM002/M, ThorLabs, USA). The scanned beam is focused on the sample by a scan lens (Model LSM05, f = 110 mm, ThorLabs, USA) after being passed through a dichroic mirror (Model DMSP805, ThorLabs, USA) that combines the OCT IR light path (1310 nm) and the HSI visible light path (400-800 nm). The beam coming back from the sample passes backwards through the dichroic mirror, the scan lens and the OCT-scanning engine, and enters back into the sample arm of the interferometer. The combined sample and reference arms signals forming an interference pattern are directed to the OCT spectrometer (COBRA SWIR OCT Spectrometer of Wasatch Photonics, USA,) through the third port of the fibre circulator. The signals acquired by the spectrometer are digitized by a frame grabber (PCI 1430 of National Instruments, USA) and processed to extract the depth-resolved reflectivity profile of the sample. A dedicated LabVIEW-based executable software, developed by Physical Sciences Inc., USA,) controls the SDOCT instrument and processes the acquired data [22, 23]. Thus, cross-sectional images of the sample are obtained with a frame rate of 20 to 60 images/sec, depending on the size of the image.
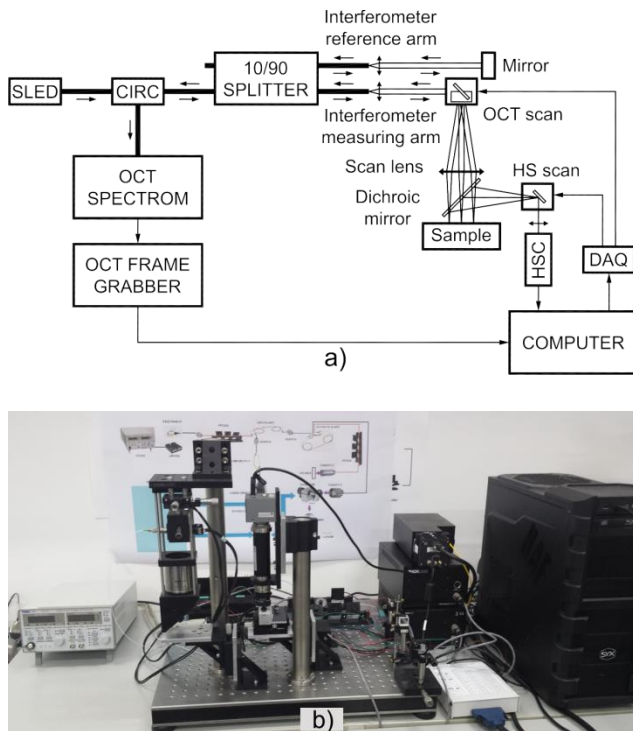

Fig. 4. Dual-mode surgery guidance system: (a) simplified diagram and (b) experimental setup.

HSI subsystem uses a hyperspectral camera HSC (PS-FW-11-V10 from Specim, Finland) which consists of a CCD camera and a spectrograph (see Fig. 3). The hyperspectral camera is similar to that described in [19], which we used for assessing mammary tumours, but was implemented to share a common path with SDOCT subsystem. A scanning mirror (1D-galvanometer GVSM001/M from ThorLabs, USA) is used to scan the sample. This scanner is controlled by the same DAQ (PCI 6251 DAQ from National Instruments, USA) used to control the OCT scan.

The hyperspectral images are acquired by the same LabVIEW-based software and processed in ENVI 5.1 (Exelis VIS, USA).

2.3. Dual-mode surgery guidance system testing

2.3.1. Samples

To explore the potential of dual-mode SDOCT-HSI system to identify the tumour boundaries, a rat rhabdomyosarcoma sample was made available by the veterinary specialist MD. Raluca Negreanu at University of Agronomic Sciences and Veterinary Medicine, Faculty of Veterinary Medicine, Bucharest. All experimental studies were conducted under the supervision of MD. Raluca Negreanu.

2.3.2. Acquisition of SDOCT and HSI images

The SDOCT and HSI images from the same location of the sample are acquired by sharing the optical path, as seen in Fig. 5). A dichroic mirror transmits the infrared light from SDOCT subsystem and reflects the visible light to the HSI subsystem.

The HSI subsystem has its own scanning mirror, which allow to explore the sample line by line by simply rotating the mirror.
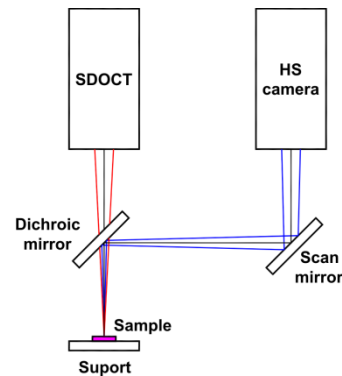

Fig. 5. Acquisition of SDOCT and HSI images.

The SDOCT subsystem scans the sample using a 2D scanning mirror system and an f-theta scan lens, as shown

in Fig. 3. The scanning lens was chosen to have a large effective focal length and a working distance large enough (100 mm) to allow for the use of a large dichroic mirror. The fields of view of the two subsystems were made identical and their scanning engines were synchronized to enable temporal co-registration of the acquired data.

Both the OCT and the hyperspectral images are acquired simultaneously. A dedicated LabVIEW-based executable software, (see instrument GUI in Fig. 6 and block diagram detail in Fig. 7) and is used to collect spatially and temporally co-registered OCT and HS images. The instrument GUI enables instrument setup, such as the setting of the scanning parameters, the size of the SDOCT /HSI frames, and the selection of the directory for data storage.
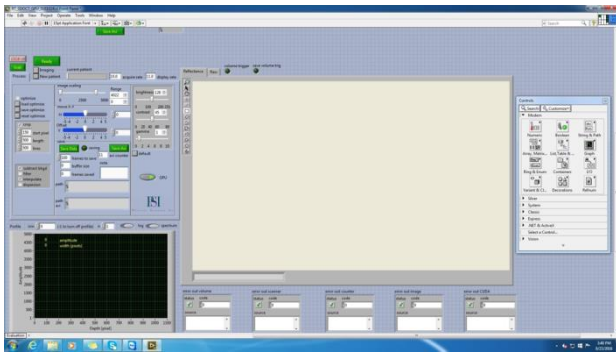

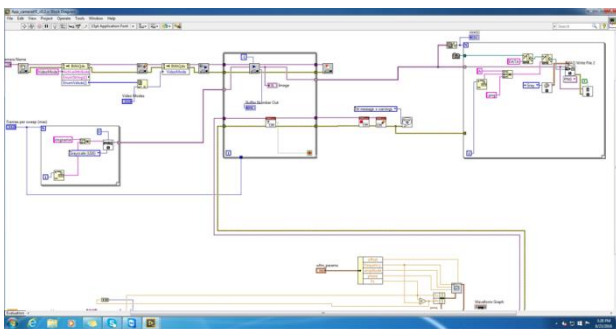*Fig. 6. SDOCT analysis software. Instrument GUI.*

Fig. 7. SDOCT analysis software. Block diagram detail.

The OCT data are processed and displayed in real-time, while the HSI data are processed in ENVI. Real-time processing of HSI data is a bit more challenging and will be implemented within the near future.

2.4. Image Processing and Analysis Methods

2.4.1. Hyperspectral Image Processing and Analysis

The processing and the analysis of the sample hyperspectral images involves the following steps:
a) elimination of redundant elements in the scene (background, areas that do not provide information about biological tissue) by selecting only a region of interest (ROI) and masking the outside pixels (Fig. 8).
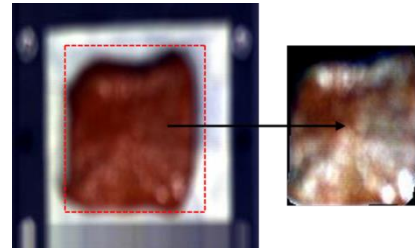

Fig. 8. Selection of the ROI.

b) determination of the inherent dimensionality of HSI image data and the noise reduction in data using the different transformations implemented in ENVI software v 5.1 such as: principal component analysis (PCA) [24], minimum noise fraction (MNF) transformation [25], independent component analysis (ICA) [26], Gabor filter [27], etc. In some applications two or more of these methods have been combined in order to extract more accurate features. In this study minimum noise fraction (MNF) transformation was considered as suitable for the determination of the inherent dimensionality of image data.

c) hyperspectral image analysis using different supervised classification methods (minimum distance, Mahalanobis distance, maximum likelihood, spectral angle mapper, binary encoding, neural network, support vector machine, etc.) or unsupervised classification method (ISODATA and K-means) [28].

To extract information about the tumour boundaries we used the spectral angle mapper (SAM) that is available in most image processing software packages [29]. This step results in a classification of the image pixels that can be used to segment the image into different areas such as for example tumour area.

2.4.2. SDOCT Processing and Analysis

A complex processing scheme is used to differentiate tissue types by analysing all the 1024 reflectivity profiles from each image [22]. The processing scheme processes each reflectivity profile (Axial-line or A-line) and derives a set of four parameters based on signal intensity and variance directly from the reflectivity profile, as well as a set of two parameters from the Fourier analysis of this signal. Then, the slope of the reflectivity profile is calculated. Linear fitting is performed on several windows, each window corresponding to a portion of the depth reflectivity profile that has the same slope. When different slopes are found within the same A-line, all the subsequent parameters are calculated in each window that was found in this initial step of the signal processing algorithm. More details may be found in [22].

The instrument GUI enable instrument setup, such as the setting of the scanning parameters, the size of the SDOCT /HSI frames, and the selection of the directory for data storage.

3. Results

The first stage of the image processing is to get SAM classification. The results derived from analysis of HSI image of rat rhabdomyosarcoma sample show (Fig. 9) a clear demarcation between tumour tissue (red area) and normal tissue (green area). The yellow line marks the frame of SDOCT scan presented later in Fig. 11.
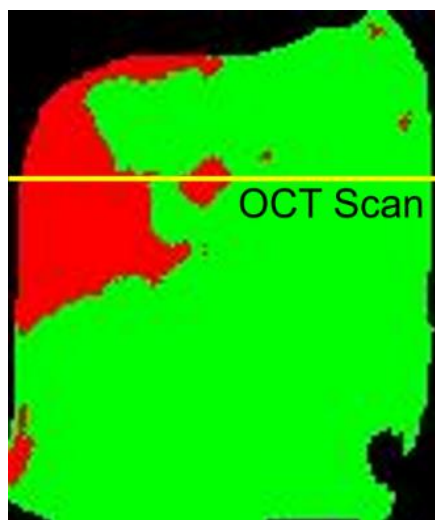

Fig. 9. SAM class results.

The two classes (tumour tissue (1) and normal tissue (2)) depicted in the SAM class map (Fig. 9) present different spatial distributions (Fig. 10 a and b) and spectral signatures (Fig. 10 c).

The image of the sample processed obeying the two rules (Fig. 10 a and b) shows that there are also parts of other classes, but they weren't taken into account because they have no relevance for tumour tissue recognition.

Thus, the HSI method permits to locate individual tissue types (tumour and normal) by their spectral signature.

One limitation of the HSI is that it does not allow to determine the depth extent of the tumour. Therefore, when combined with SDOCT, the depth spreading of the tumour can be retrieved from the SDOCT image, as shown in Fig. 10. As observed, the denser highly scattering area is caused by the densely packed cancerous cells with increased size nuclei. Similarly, a false colour map can be obtained for the SDOCT image when a tissue differentiation algorithm is used (see Fig. 11 b). As observed, the location of the tumour areas is well depicted. The tumour area is slightly oversized, both in depth and

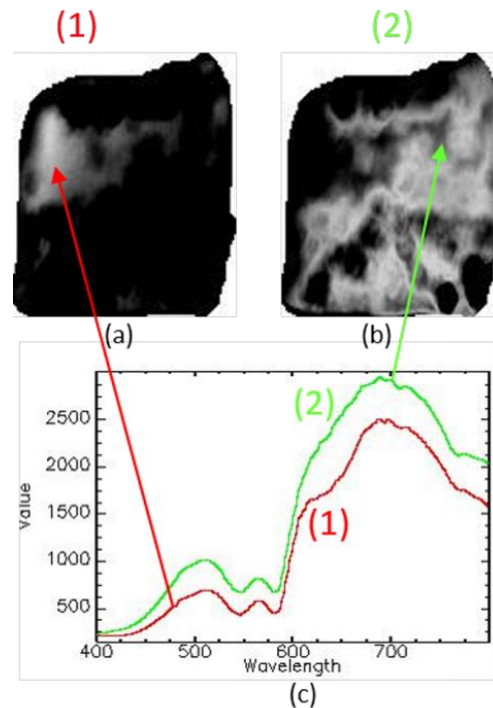laterally due to the averaging algorithm used to smooth out the image.

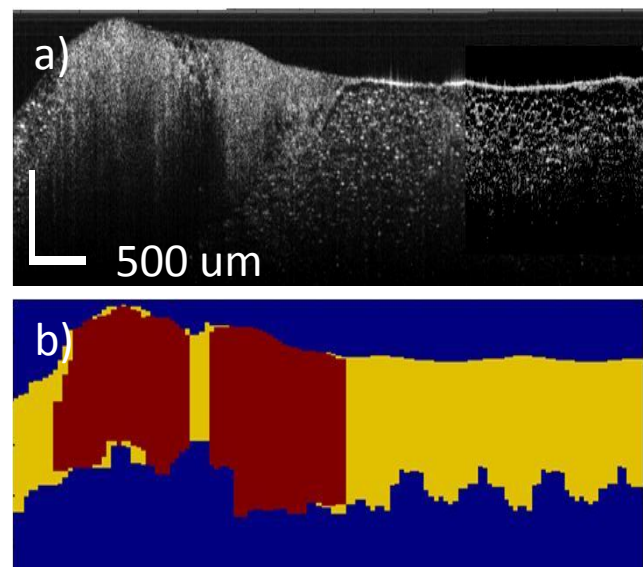*Fig. 10. SAM Rule Images. a) tumour tissue; b) normal tissue; c) spectral signature.*

Fig. 11. A frame of SDOCT scan. Tumour area delimited by red line.

This example clearly demonstrates that the complementary capabilities of OCT and HSI can be used to locate positive margins on surgical specimens. HSI retrieves the boundaries of the tumour tissue in a horizontal plane, while the depth spreading is retrieved by

SDOCT scan. OCT also serves as a confirmatory tool for cancer presence, since it clearly shows tissue morphological changes.

4. Discussions

We have combined hyperspectral imaging with SDOCT to create a tool that can dynamically and non-invasively determine tumour boundaries on excised surgical specimens. Although both techniques were used before separately for similar purposes, their combination into a single instrument was not yet demonstrated. This combination of both techniques within a single instrument has clear benefits. HSI can rapidly locate cancer presence on specimen's surface, with high specificity, but hidden cancer foci larger than 5 mm may not be always found due to HSI limited depth capability. SDOCT adds the benefit of depth localization with 2 mm from surface, and thus can provide a clearer picture of cancer spreading, but it is not 100 % specific. Therefore, the combined use of SDOCT and HSI may substantially improve both sensitivity and specificity on locating positive margins on surgical specimens.

5. Conclusions

In conclusion, the dual mode optical instrument proposed in this paper clearly has the capability to improve cancer surgery success rate. Our preliminary study suggests that the combined use of SDOCT and HSI can reliably detect positive surgical margins.

We consider that these combined techniques may be used in the future for guiding the surgeon while performing the surgery. The excised specimen can be rapidly analysed and a determination of positive margins presence may be made during the surgical operation. Improved localization of positive margins during surgery act will positively impact surgery outcome and could reduce the chances for cancer recurrence.

By this approach the surgeon can see the exact boundaries of a tumour, both in depth and in horizontal plane. SDOCT technique provides 'topography' of a tissue region while HSI gives information about its nature. Thus the guidance information is much improved.

References

[1] G. P. Swanson, K. Rynearson, R. Symmonds, Am. J. Clin. Oncol. **25**, 438 (2002).
[2] F. Meric, N. Q. Mriza, G. Vlastos, T. A. Buchholz, H. M. Kuerer, G. V. Babiera, S. E. Singletary, M. I. Ross, F. C. Ames, B. W. Feig, S. Krishnamurthy, G. H. Perkins, M.D. McNeese, E. A. Strom, V. Valero, K. K. Hunt, Cancer **97**, 926 (2003).
[3] A. W. Dick, M. S. Sorbero, G. M. Ahrendt, J. A. Hayman, H. T. Gold, L. Schiffhauer, A. Stark, J. J. Griggs, J. Nat. Cancer Institute **103**, 92 (2011).
[4] L. Jacobs, Ann. Surg. Oncol. **15**, 1271 (2008).
[5] S. L. Blair, K. Thompson, J. Rococco, V. Malcarne, P. D. Beitsch, D. W. Ollila, J. Am. Coll. Surg. **209**, 608 (2009).
[6] E. K. Valdes, S. K. Boolbol, J. M. Cohen, S. M. Feldman, Ann. Surg. Oncol. **14**, 1045 (2007).
[7] K. Satoh, T. Kobayashi, Y. Kawase, M. Mitani, K. Takahashi, H. Takashima, M. Ohkawa, M. Tanabe, K. Kojima, Radiat Med. **14**, 167 (1996).
[8] M. Toepker, C. Czerny, H. Ringl, J. Fruehwald-Pallamar, F. Wolf, M. Weber, O. Ploder, C. Klug, Oral Oncol. **50**, 221 (2014).
[9] I. M. Obdeijn, M.M. Tilanus-Linthorst, S. Spronk, C.H. van Deurzen, C. de Monye, M. G. Hunink, M. B. Menke, AJR Am. J. Roentgenol. **200**, 304 (2013).
[10] G. J. Spicer, M. Kazim, L. R. Glass, G. J. Harris, N. R. Miller, J. Rootman, T. J. Sullivan, Ophthal. Plast. Reconstr. Surg. **29**, 277 (2013).
[11] T. Karni, I. Pappo, J. Sandbank, O. Lavon, V. Kent, R. Spector, S. Morgenstern, Sh. Lelcuk, Am. J. of Surgery **194**, 467 (2007).
[12] D. Huang, E.A. Swanson, C.P. Lin, J. S. Schuman, W. G. Stinson, W. Chang, M. R. Hee, T. Flotte, K. Gregory, C. A. Puliafito, J. G. Fujimoto, Science **254**, 1178 (1991).
[13] N. Ramanujam, Neoplasia **2**, 89 (2000).
[14] G. Lu, L. Halig, D. Wang, Z.G. Chen, B. Fei, Proc. SPIE Int. Soc. Opt. Eng. **12**, 9036:90360S (2014).
[15] H. Akbari, L.V. Halig, D.M. Schuster, A. Osunkoya, V. Master, P. T. Nieh, G. Z. Chen, B. Fei, J. Biomed. Opt. **17**, 076005 (2012).
[16] L. Zhi, W. Hongjun, L. Qingli, Sensors, **12**, 162 (2012).
[17] G. Lu, B. Fei, J. Biomed. Opt. **19**, 010901 (2014).
[18] M. A. Calin, S. V. Parasca, D. Savastru, D. Manea, App. Spect. Reviews **49**, 435 (2014).
[19] D. Manea, M. A. Calin, S. Miclos, D. Savastru, R. Negreanu, Rom. Rep. Phys. **67**, 1503 (2015).
[20] J.S. Schuman, Trans. Am. Ophthalmol. Soc. **106**, 426 (2008).

[21] A. F. H. Goetz, G. Vane, J.E. Solomon, B.N. Rock, Science **228**, 1147 (1985).

[22] D. Savastru, E. W. Chang, S. Miclos, M. B. Pitman, A. Patel, N. Iftimia, J. Biomed. Opt. **19**, 056001 (2014).

[23] N. Ukhrowiyah, D. Kurniadi, Suhariningsih, M. Yasin, Optoelectron. Adv. Mat. **9**, 995 (2015).

[24] R. Gonzalez, R. Woods, Reading, Massachusetts, Addison-Wesley Publishing Company, 1993, p. 148.

[25] A. A. Green et al., IEEE Trans. Geosci. Remote Sens. **26**, 65 (1988).

[26] J. M. P. Nascimento, J. M. B. Dias, IEEE Trans. on Geoscience and Remote Sensing **43**, 175 (2005).

[27] L. Liu, M. Ngadi, S. Prasher, C. Gariépy, J. Food Eng. **99**, 284 (2010).

[28] D. Lu, Q. Weng, Int. J. Remote. Sens. **28**, 823 (2007).

[29] F. A. Kruse, A. B. Lefkoff, J. B. Boardman, K. B. Heidebrecht, A. T. Shapiro, P. J. Barloon, A. F. H. Goetz, Remote Sensing of Environment **44**, 145 (1993).

_____

[*]Corresponding author: miclos@inoe.ro